Research Paper

# Measurements of absolute atomic oxygen density by two-photon absorption laser-induced fluorescence spectroscopy in hot air plasma generated by microwave resonant cavity

---

## ABSTRACT

Hot air plasma is generated inside a 2.45GHz microwave resonant cavity and is ejected towards a gas conditioning cell at 600 mbar. A flow of 12 liter/min of dry air with a small amount of $H_2$, in order to better detect OH(A-X) spectra for gas temperature measurements, is injected at the entrance of the resonant cavity using an input power of 1 kW. The measurement of absolute density of atomic ground state oxygen is determined using two-photon absorption laser-induced fluorescence (TALIF) spectroscopy for several radial and axial positions of the hot air plasma column which is a post discharge propagating inside the cell. The gas temperature corresponding to the radial and axial positions, where atomic oxygen density is measured, varies between about 3500K in the column axis down to about 2500K in the plasma border. The measured absolute oxygen density using xenon for calibration varies between about $2.1 \times 10^{17} cm^{-3}$ in the axis down to $0.05 \times 10^{17} cm^{-3}$. This leads to a dissociation degree of oxygen inside the post discharge air plasma column lower than the case where only local thermodynamic equilibrium is assumed. This deviation is due to non-thermal equilibrium effects that can be associated to the not yet achieved relaxation of the long-lived excited species during such post discharge stage.

*Keywords: non-thermal microwave air plasmas, density of atomic oxygen, two-photon absorption laser-induced fluorescence, oxygen dissociation, gas temperature measurement*

# 1. INTRODUCTION

Many applications and understanding of plasma physics can be reached using the present hot air plasma generated by the microwave resonant cavity. In our case, the experimental characterization to obtain more particularly the density of atomic oxygen in such air plasma is intended to be used for validation of a complex hydro-kinetics model involving transport and plasma chemistry.

Optical emission spectroscopy (OES) usually gives direct access to the radiative excited species in order to get the absolute densities of only the emissive species (species of the upper level of the transition) provided the emission spectra is calibrated using a spectral lamp. OES gives also information on for instance the temperatures of gas, rotation and vibration species from classical comparison between synthetic and experimental specific molecular spectra. However, OES cannot directly give any information on the non emissive states as the density of the atomic ground state density which can exceed the excited species by several orders of magnitude in the case of our microwave plasmas.

The alternative to obtain the atomic oxygen density of the atomic ground state in the present microwave hot air plasma is to use the absorption spectroscopy and more particularly the laser-induced fluorescence spectroscopy (LIF) that generally gives direct access to the density of the non emissive species as atomic ground states and also metastables.

It has been used in the present work a two-photon absorption laser-induced fluorescence (TALIF) spectroscopy to measure the absolute atomic oxygen density in the hot air plasma generated by a microwave resonant cavity. The principle of this laser diagnostic to measure the absolute density is already described in an abundant literature more particularly in the case of low temperature plasmas. The reader can see for instance [1] and the references given therein that describe in details the laser-induced fluorescence spectroscopy and its advantages in comparison for instance to standard absorption or Raman spectroscopy.

It is important to note in the case of the measurements of atomic oxygen density that TALIF spectroscopy has been used in the literature in several setups of low temperature plasmas generated for instance by pulsed microwave source of SLAN type [2] or by RF plasma jet at atmospheric pressure using helium gas flow [1], or by pulsed dielectric barrier discharge in air [3], and also pulsed corona discharge in air [4], or by high voltage source at high frequency using Argon flow for generation of atmospheric pressure plasma jet [5] and many other recent references in the case of low temperature plasma jets at atmospheric pressure. It is also interesting to note another measurement [6] of absolute density of ground state of atomic oxygen based a visible cavity-enhanced absorption spectroscopy in the case of lower pressure plasma (20 Torr) generated by an ICP (induced capacitive plasma) reactor.

However, TALIF and absorption spectroscopy was never used in the case of hot air plasma generated by a microwave resonant cavity.

Section 2 following this introduction is devoted to the description of the experimental setup used to generate the hot air plasma from microwave resonant cavity and also the laser setup of TALIF spectroscopy used to measure the absolute density of atomic oxygen. In section 3, the TALIF method and formalism are described together with the method of the calibration that is based on a comparative TALIF measurement with xenon. The obtained results are then discussed and analyzed.

# 2. EXPERIMENTAL SETUPS

## 2.1 Microwave source for hot air plasma generation

The experimental setup is shown in figure 1. Microwave power is provided by a 2.45 GHz magnetron source (manufactured by Sairem) allowing power output variation up to 3 kW. The microwave radiation generated by the magnetron is guided through a waveguide system including a circulator (enveloped by a water load for the thermal protection of the magnetron head with a water cooling system), a tapered waveguide (WR-340) and a resonant cavity for microwave plasma generation. The above system is terminated by a movable short circuit sliding which allows the maximum field at the launcher position. Plasma ignition is achieved through a spark discharge applied in the down side of the resonant cavity. The plasma microwave power $P_{MW}$ is determined as $P_{MW}=P_I - P_R$, where $P_I$ and $P_R$ are the incident and reflected microwave powers, respectively. These incident and reflected microwave powers are directly displayed by the microwave generator in order to minimize the lost reflected power (not used to generate the plasma) using the short circuit sliding. The flow of hot air plasma (plasma column displayed in figure 2) exits out the upstream side of the resonant cavity in a sealed cell (1 liter of volume) made of stainless steel. This gas conditioning cell is equipped with synthetic fused silica windows which is transparent to a wide range of wavelengths from UV to IR (about 200 nm up to 2000 nm) in order to be used for the spectroscopy and also the naked eye observation of the hot air plasma. The cell is also equipped with a pumping system using a rotary vane vacuum pump (Adixen PASCAL C2 Series) allowing for the present setup a working pressure range between 50 mbar to 1000 mbar. Furthermore, the external walls of this sealed cell are cooled in order to suppress thermal damage of more particularly the upper part of the cell which is in contact with the top of the plasma column. Both sides of the microwave resonant cavity are equipped with special windows to keep pressure constant in the resonant cavity and in the cell. The gas inlet (e.g. Air or Air and Hydrogen mixture) is injected from below the microwave resonant cavity by using a Brook mass flow meter SLA5850S (maximum flow rate 30 l/min) controlled by Brooks 0254 controller. To keep the cell pressure constant during the measurement an automatic pressure control is used. This pressure controller involves a PID controller system, a control valve placed in the input side of the primary pump and a pressure measuring system. The regulator controls the opening and closing of the control valve to regulate the pressure in the cell until reaching the desired pressure.

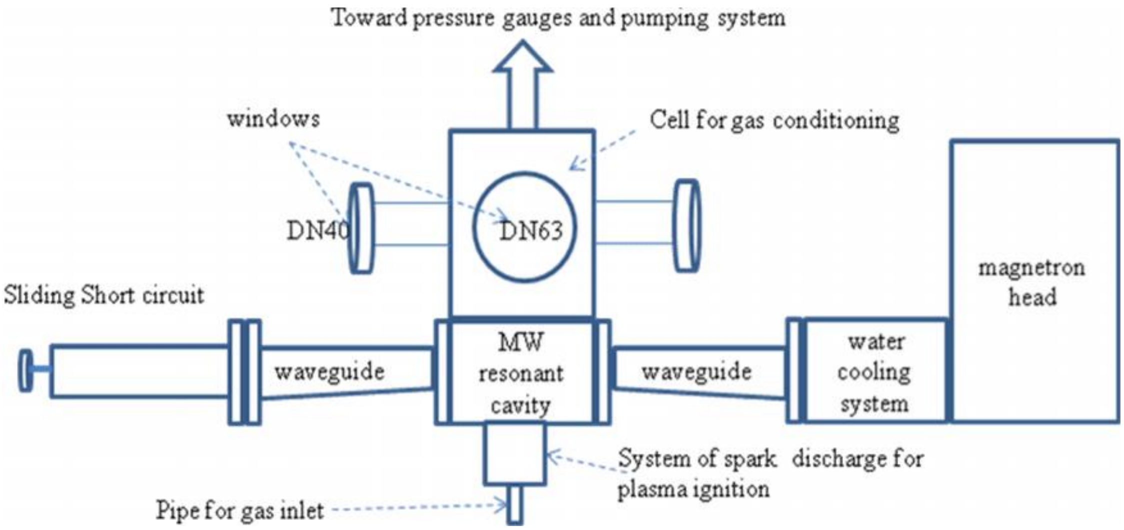

**Fig. 1. Schematic view of the experimental setup including the microwave resonant cavity with gas conditioning cell and the 2.45GHz microwave generator with a magnetron head and a power supply not shown in this scheme**.

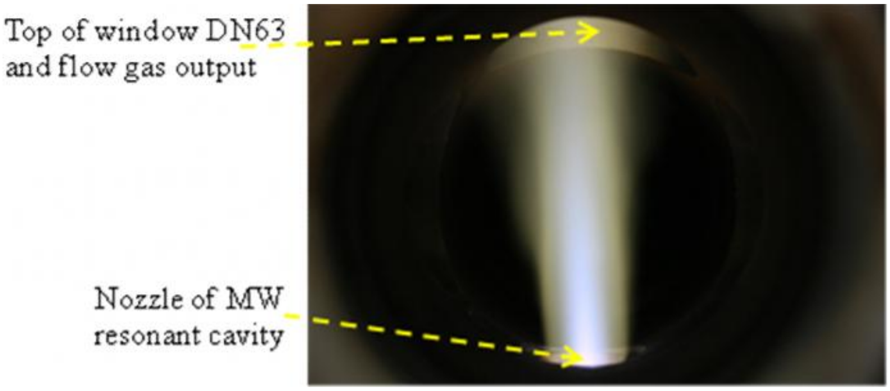

**Fig. 2. Air plasma column inside the cell for $P_{MW}$ = 1kW, Air gas flow=12 l/min and pressure=600 mbar**.

Light emitted by the plasma column is collected perpendicularly to the plane of the scheme of figure 1 through DN63 window using a lens (x2 magnification) mounted on a sliding stand to perform a scan along the radial and axial direction of the plasma column. The emitted radiation is guided into the entrance slit (wide=100 μm) of the spectrophotometer (0.75m V MC: Acton Spectra Pro 2750i, in the Czerny–Turner configuration) via a 3m long optical fiber (OF: UV-Silicon LG-455-020-3). The detecting device is CCD camera (CCD: PIXIS -100, 256 × 1024 Imaging array 20 $\mu$m × 20 $\mu$m pixels) placed at the exit port of the spectrophotometer. The spectral domain lies within 200nm and 920nm. The spectrum is recorded without any correction for the wavelength dependence of the relevant detection device. For UV emissions (i.e. 200nm to 400nm) a grating of 2400 grooves/mm is used and air is a natural high-pass filter. For 400nm to 900nm spectral ranges we used a grating of 1800 grooves/mm, with a high-pass filter being either the Corning 0-53 (cutting wavelength at 340 nm) or the MTO J517a (cutting wavelength at 517 nm). The two gratings of 1800 grooves/mm and 2400 grooves/mm provide a spectral resolution of the spectrophotometer close to respectively 0.02 nm and 0.015 nm.

## 2.2 Experimental setup for TALIF diagnostics

Figure 3 displays the schematic diagram of experimental setup used for two-photon absorption laser-induced fluorescence (TALIF) spectroscopy to measure the absolute density of atomic oxygen. A dye laser (Sirah Strech-Cobra) pumped by a Nd:YAG laser (Quanta Ray CGR 150, max pulse energy of 180 mJ) provided 7 ns pulse width with a repetition rate of 30 Hz. The spectral width of the laser radiation in the range between 435nm to 463nm, measured using two 1800 grooves/mm gratings, amounts to 1.7 pm. The maximum pulse energy of the dye laser beam is about 20 mJ per pulse. The second harmonic of laser beam is generated by a nonlinear BBO crystal to obtain a wavelength range of 220 nm to 230 nm with a spectral width of 2 pm that allows us to excite the two-photon transition from the ground states of the triplet atomic oxygen $2p^4$ $(3P)_{J=0,1,2}$ to the excited states 3p $(3P)_{J=0,1,2}$ of atomic oxygen. The beam diameter is 2 mm and the pulse energy up to 0.2 mJ. The laser beam is focused at a given position of the plasma column using a $MgF_2$ lens with a focal length of 170 mm.

The TALIF fluorescence is detected perpendicularly to the incident laser beam. The laser focus is imaged onto the photocathode of a photomultiplier (PMT HamamatsuH7421-50) working in a single photon counting mode, by using BK7 lens with the ratio f/D=75/25 (i.e. 75 mm focal length over 25 mm diameter). The size of the image is limited by a diaphragm placed in the focal plane in front of the photomultiplier. A second diaphragm (1 mm diameter) is placed between the lens and the cell in order to reduce the flux of fluorescence. The anode pulses delivered by the PMT are delayed via a delay line and then processed via a constant fraction discriminator (CFD). The number of photons is stored in a multi-channel Stanford Research SR-430 analyzer set having 16 384 channels and 5ns resolution. For each laser pulse, the SR 430 is monitored by fast photodiode. Further details on the laser setup and the electronic recording devices from photo-multiplier to multi-channel analyzer can be found elsewhere [7].

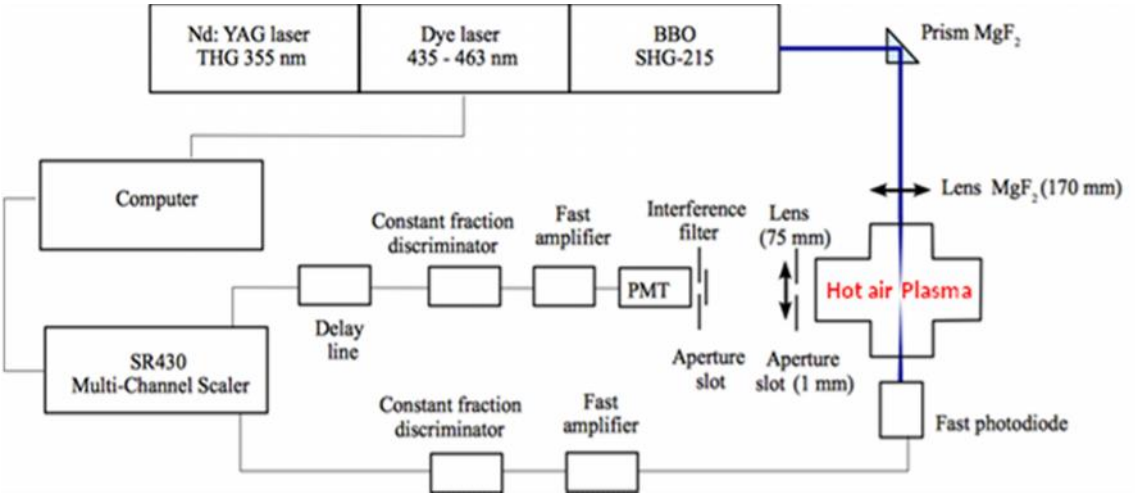

**Fig. 3. Schematic view of the experimental setup for TALIF diagnostics used for measurement of Oxygen atom**.

# 3. RESULTS AND DISCUSSION

## 3.1 TALIF spectroscopy

Laser radiation is focused into a given position of the air column plasma where the measurement of the atomic oxygen O density is required. As the excitation of O needs VUV photons (10.98 eV) which are sophisticated to generate due to the complexity of VUV spectroscopy and strongly absorbed at higher pressure, it is more practical to replace single VUV photon by two UV photons (i.e. TALIF). In that case, the excitation of ground state of atomic oxygen takes place by the simultaneous absorption of two photons. The first photon excites the atom into a virtual state with a very short lifetime (about $10^{-16}$s) and the second one have to be absorbed within this lifetime to provide the required excitation of the real state. This means that the collision cross sections of two photon excitation are lower than the single-photon excitation by several orders of magnitude; a high photon flux is therefore required for two-photon excitation of atomic oxygen. When the high photon flux condition is fulfilled, the most dominant excitation process by the two photons is the induced absorption leading to the excitation of the upper level of the fluorescent transition of excited atomic oxygen. However, the effect of competing process populating the considered excitation (as cascades from higher level or electron impact excitation, etc.) has to be considered carefully since they may not be negligible. Furthermore, as it is discussed afterwards in this section, the depopulation of the excited atomic oxygen is ideally dominated by fluorescence process that can compete with quenching processes (collision de-excitation) or photo-ionization.

## 3.2 Absolute density measurement of ground state of atomic oxygen

Figure 4 summarizes the pathways of two photon excitation of atomic oxygen from the triplet ground state and also of xenon used for density calibration. The fluorescence from both the triplet excited state of 3p $^3P_{j=1,2,0}$ and excited xenon state 6p'[3/2] is also shown.

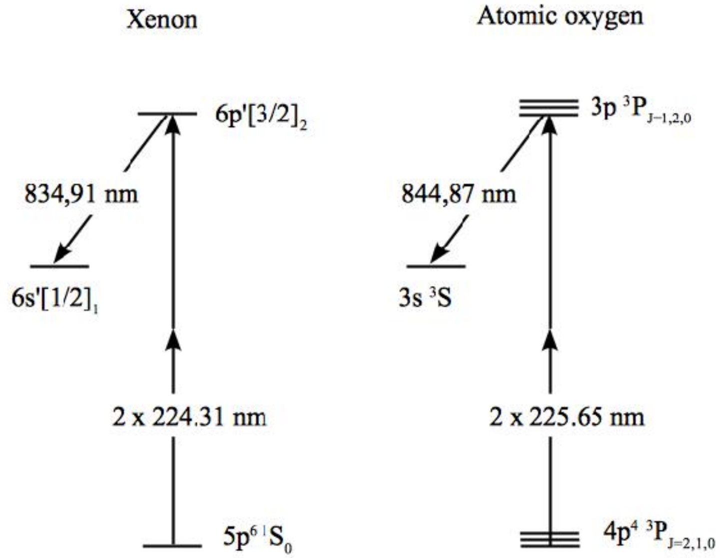

**Fig. 4. Two-photon excitation schemes of atomic oxygen and xenon related to the determination of absolute atomic ground state densities using xenon as a reference for TALIF calibration.**

The determination of the absolute atomic oxygen density was performed following two steps. In the first step the calibration measurement was achieved at one spatial position corresponding to r=0mm for the radial position from vertical axis of the torch and z=12mm from the nozzle of the microwave resonant cavity (zero axial position). This position corresponds to the lowest z value that is possible to consider since the laser beam is introduced inside the cell through the DN40 window shown in figure 1. In the second step, the TALIF signal was measured as a function of the radial position at axial distance z= 17 mm.

### 3.2.1 Calibration and TALIF formalism

The oxygen TALIF spectrum (figure 5) was recorded when the laser beam is focused into the center of the cell for an exciting laser wavelength ranging from 225.4 nm to 226.4 nm. The fluorescence at 845 nm is detected by the photomultiplier through an interferential band pass filter (having a full width at half maximum FWHM = 10 nm). The fluorescence photons were collected during 600 laser shots and the number of photoelectrons detected per laser pulse (pulse duration less than 7 ns) does not exceed one photon per pulse to fulfil the single photon counting condition. Thus, the fluorescence intensity is normalized to a square energy of 1$\mu$J$^2$ and one laser pulse.

The three excitation lines peaking at 225.655 nm, 226.090 nm and 226.262 nm are well identified as two-photon absorption of the J = 2, 1, 0 levels of atomic oxygen ground state.

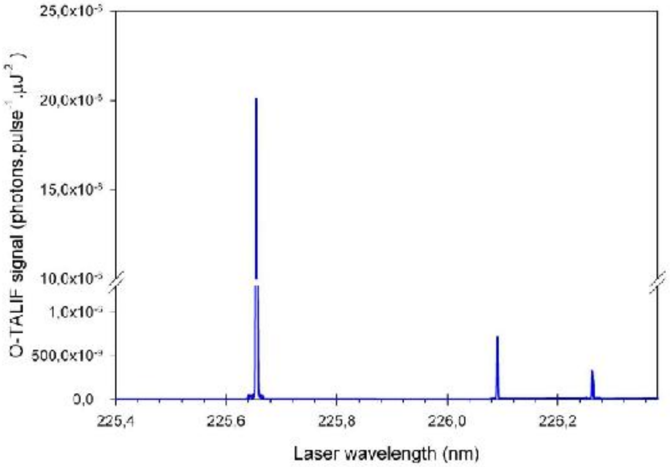

**Fig. 5. Two-photon excitation spectrum of atomic oxygen (emission wavelength: 845 nm) recorded in the plasma column in the center of the cell at 600 mbar, Air flow= 11.64 L/min, $H_2$ flow= O.36 L/min, $P_{MW}$ = 1 kW .**

The fine structure and the line profiles of the three components of the two-photon excitation spectrum are displayed figure 6. It is noteworthy that the fine structure of the components corresponding to the excitation of the triplet states 3p $3P_0$, 3p $3P_1$ and 3p $3P_2$ cannot be clearly resolved due to the very low energy range (not exceeding 0.7 $cm^{-1}$) between these excitation levels. This energy range corresponds to an excitation laser wavelength interval up to 0.6 pm. The Gaussian profile of the laser beam (FWHM = 2pm) do not allow us to separate the different components of this fine structure.

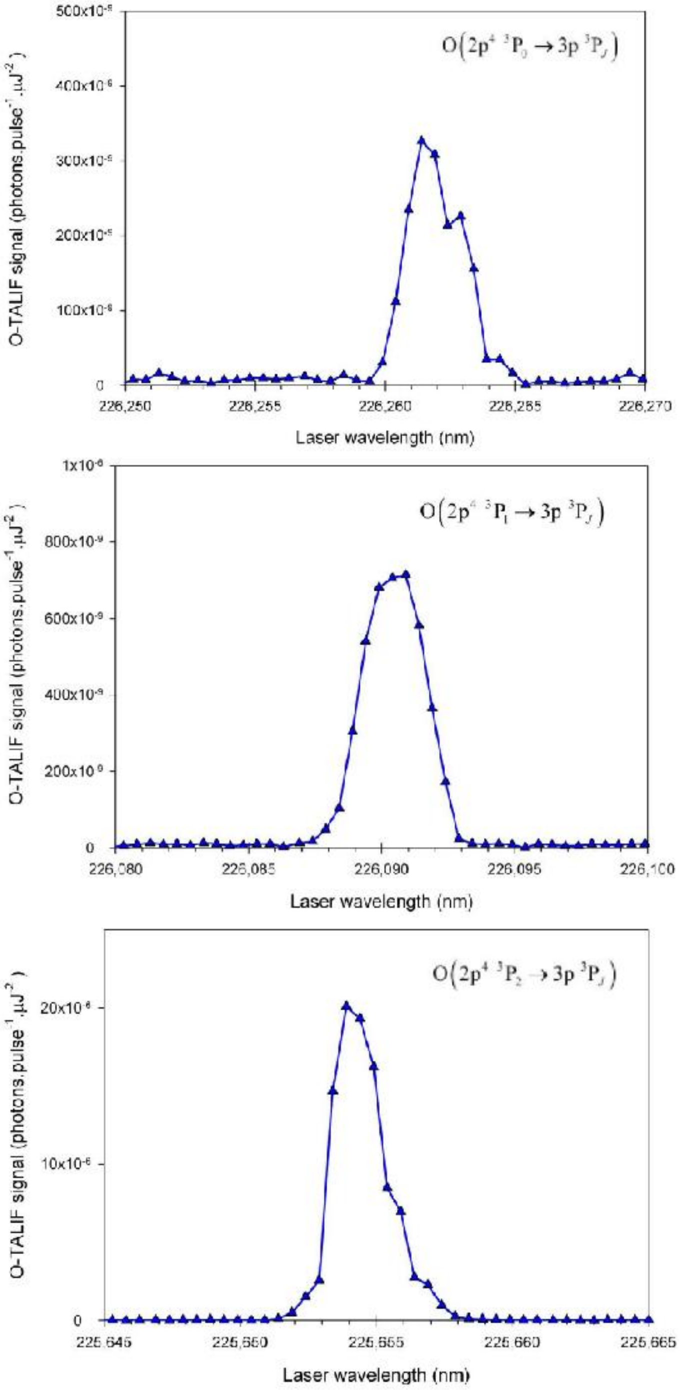

**Fig. 6. Two-photon excitation line profiles of the $O(2p^4\ ^3P_{0,1,2} \rightarrow 3p\ ^3P_J)$ transitions obtained in the plasma column in the center of the cell at 600 mbar, Air flow= 11.64 L/min, $H_2$ flow= O.36 L/min, $P_{MW}$ = 1 kW**

The fluorescence signal is obtained by integrating the line profile of the lower three sub-levels ($2p^4\ ^3P_2$) over the excitation wavelengths and by normalizing to the square of energy and to one laser pulse. The very low intensity of the TALIF signals arising from the other transitions lines $O(2p^4\,{}^3P_{1,0} \rightarrow 3p\,{}^3P_J)$ are too weak to be taken into account. The line shape of the two-photon transition $O(2p^{4\,3}P_2 \rightarrow 3p\,{}^3P_J)$ can be fitted by a Gaussian profile mainly resulting from the Gaussian contribution of 2 pm bandwidth laser contribution. The Lorentzian contribution due to the pressure broadening is not significant in the plasma column (figure 7) and the FWHM of the line is quite independent of the pressure. The discrepancy between the FWHM of laser beam (about 2 pm) and the FWHM measured (3 pm) is weak. It is probably due to the fine structure of the excitation spectrum. Thus, the fluorescence intensity spectrally integrated corresponds to the excitation of the upper three sub-levels.

The shift of the line position cannot be evaluated with enough accuracy. The wavelength reproducibility of the dye laser beam is up to 5 pm. So the line shift can be mainly attributed to the random error of the measured wavelength in view of the uncertainty of the wavelength calibration.

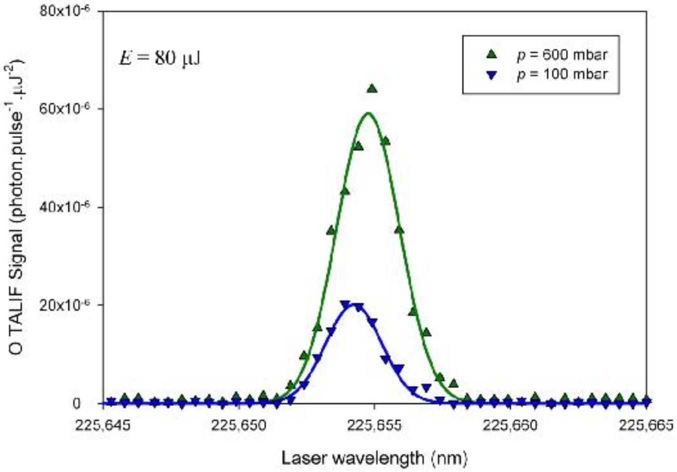

**Fig. 7. Two-photon line profiles of the $O(2p^4\,{}^3P_{0,1,2} \rightarrow 3p\,{}^3P_J)$ transitions obtained in the plasma jet at two different pressures. (Air flow= 11.64 L/min, $H_2$ flow= 0.36 L/min, $P_{MW}$ = 1 kW) .**

Figure 8 shows the spectrally integrated and normalized to one laser pulse TALIF signal obtained in the plasma column as a function of the laser pulse energy.

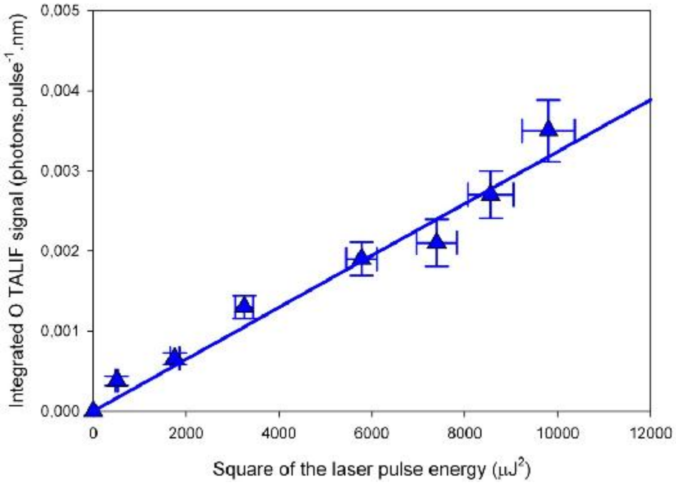

**Fig. 8. Integrated O TALIF signal versus the square of the laser pulse energy at 600 mbar, Air flow= 11.64 L/min, $H_2$ flow= 0.36 L/min, $P_{MW}$ = 1 kW**

The response of the TALIF signal is quadratic and unsaturated until the laser pulse energy reaches 100 µJ. At these low pulse laser energies, the quadratic response indicates that the TALIF measurements are carried out without saturation and photo-ionization effects. It is noteworthy that the quenching of excited O atoms by ground state O atoms can be neglected whether the atomic oxygen is lower than molecular background nitrogen and oxygen. Furthermore, the upper limit of the quenching rate constant of excited oxygen atom was estimated to be quite low ($0.82\times10^{-11}$ $cm^3/s$) in an oxygen plasma jet having a sufficiently high and controllable degree of dissociation [8]. Thus, in the present plasma column, the radiative time decay of reaction remains shorter than the collisional time decay reaction. This means that the fluorescence signal and the resulting estimation of oxygen density are not really affected by such collisionnal quenching.

In order to determine the calibration factors, the oxygen TALIF signal spectrally integrated and normalized to one micro-joule square and one pulse can be compared to the xenon TALIF signal as already done in the literature (see e.g. [1]). The fluorescence at 830 nm was recorded in the same conditions excluding the interferential filter whose transmission is different. The gas conditioning cell was filled in with xenon at static pressures (no gas flow) ranging from 1 torr to 10 torr when the microwave power is off. The xenon TALIF signal is integrated and normalized in the same way as oxygen TALIF signal. The laser pulse energy was tuned low enough, below 70 μJ, to avoid xenon ionization by one photon absorption of the two-photon excited state Xe $6p'[3/2]_2$. Beyond this energy limit, the xenon TALIF signal seems to be slightly saturated as shown in figure 9.

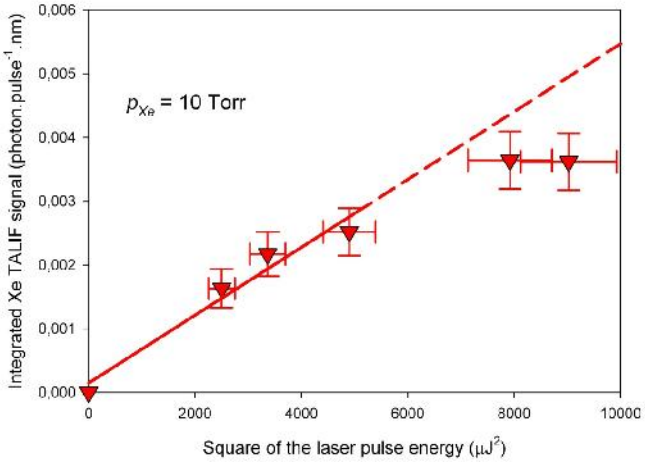

**Fig. 9. Integrated Xe TALIF signal versus the square of the laser pulse energy.**

Figure 10 shows that the normalized and integrated xenon TALIF signal is proportional to the xenon pressure and to the xenon density because the xenon calibration was achieved at constant room temperature (295 K). The linear variation of the xenon signal versus the xenon density could indicate the collision de-excitation of the Xe $6p'[3/2]_2$ state is negligible under the scanned pressure range. Nevertheless, a collision decay of the state Xe $6p'[3/2]_2$ forming Xe $6p[1/2]_0$ state cannot be excluded. The emission of Xe $6p[1/2]_0$ at 828 nm is close to the wavelength of the emission of the Xe $6p'[3/2]_2$ state at 834.7 nm and can be detected through the interferential filter used with the detection of xenon fluorescence. Anyway, the decay rate measurements of the Xe $6p'[3/2]_2$ state carried out by analysing the fluorescence decay of the emissions recorded through the interferential filter for pressure ranging from 1 torr to 10 torr do not show a significant variation of the decay rate versus the pressure (data not shown). Then the slope of the line representing the normalized xenon TALIF signal as a function of the density can be used as the calibration factor for oxygen density measurements.

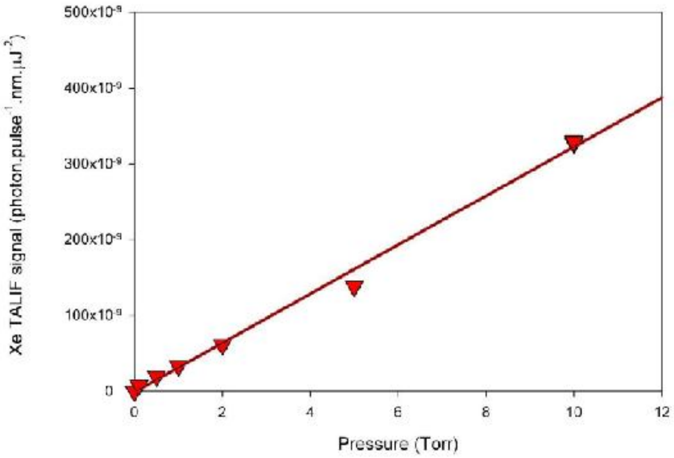

**Fig. 10. Integrated and normalized xenon TALIF signal as a function of the xenon pressure. Fluorescence recorded through an interference filter centered at 830 nm (Bandwidth = 10 nm).**

The detection sensitivity of the photomultiplier ($\eta_O$ or $\eta_{Xe}$) is nearly equal for both fluorescence wavelengths at 834.9 nm ($\lambda_L$(Xe) for xenon) and 844.9 nm ($\lambda_L$(O) for oxygen) shown in figure 4. The transmission of the interferential filters are respectively $T_{Xe}$=63% and $T_O$=81% (taken from data sheet calibration curves). According to the literature [1], the optical branching ratio for the atomic oxygen transition 3p $^3P_J \rightarrow$ 3s $^3S$ is unity (*a(O)* =1) and *a(Xe)*=0.733 for the xenon transition 6p'[3/2]$_2 \rightarrow$ 6s'[3/2]$_1$ while the two-photon excitation cross section ratio is $\sigma^{(2)}_{Xe}/\sigma^{(2)}_O = 1.9 \pm 0.4$ with $\sigma^{(2)}_{Xe} \approx 2.5 \times 10^{-35}$ cm$^4$ [9] and $\sigma^{(2)}_O \approx 1.3 \times 10^{-35}$ cm$^4$ [10].

The unknown density of atomic oxygen $n_O$ is then derived from the xenon gas density $n_{Xe}$ and the ratio $S_0/S_{Xe}$ of normalized TALIF signals measured for xenon and oxygen in the plasma column. At 600 mbar and z=12 mm from the nozzle in the axis of the plasma column, the absolute density of background level of atomic oxygen is :

$$n_O = \frac{T_{Xe}\eta_{Xe}}{T_O\eta_O}\frac{a(Xe)\sigma^{(2)}_{Xe}}{a(O)\sigma^{(2)}_O}\left(\frac{\lambda_L(Xe)}{\lambda_L(O)}\right)^2 n_{Xe}\frac{S_O}{S_{Xe}} = 0.62 \times n_{Xe} = (2.05 \pm 0.52) \times 10^{+17}\,\mathrm{cm}^{-3} \qquad (1)$$

This result shows that the molecule of oxygen $O_2$ is strongly dissociated near the nozzle since the gas temperature is high (around 3500 K as shown in section 3.3).

### 3.2.2 Radial measurement of the oxygen density

The radial zero position corresponds to the axis of the plasma column. The radial scan is achieved by a lateral and horizontal displacement of the whole cell perpendicularly to the laser beam in the opposite direction of the fluorescence detection. In fact to maintain the same optical pathway for the laser beam, the positions of the lens imaging the focal region and the photomultiplier are not changed. Therefore, the laser beam is always focused at the same distance of the nozzle of the microwave resonant cavity (z=17 mm) at a radial position from the vertical axis of the plasma column ranging from r=0 to r=5 mm. The detection conditions of the fluorescence are strictly identical for all the chosen radial positions. The direction and position of the laser beam remains unchanged during these cell displacements for the radial scan of the plasma column.

The measured radial profile of ground state atomic oxygen displayed in figure 11 follows a quasi-gaussian shape.

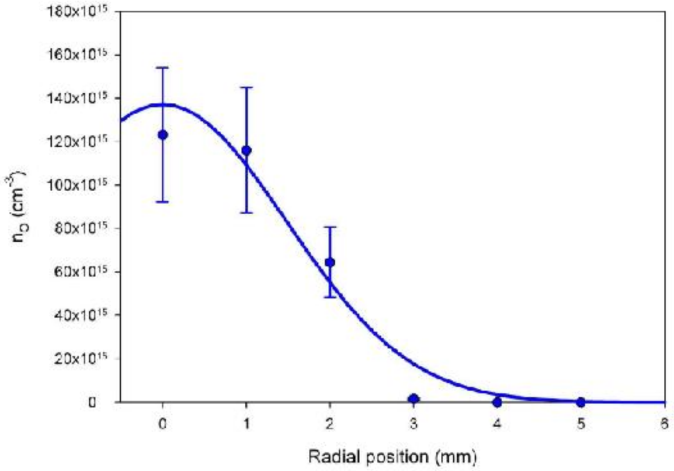

**Fig. 11. Absolute atomic oxygen density in the microwave plasma column versus radial position at z=17 mm from the nozzle of resonant cavity: pressure= 600 mbar, Air flow= 11.64 L/min, $H_2$ flow= O.36 L/min, $P_{MW}$ = 1 kW**

### 3.3 Discussion

First of all, in order to know the dissociation degree of molecular oxygen, it is necessary to determine the gas temperature for the chosen gas pressure (600mbar).

Gas temperature can obtained from OH(A-X) spectra corresponding to $OH(A^2\Sigma^+) \rightarrow OH(X^2\Pi_{3/2})$ emission bands ([11] or [12]). As previously mentioned a small amount of $H_2$ has been added in order to better detect the OH(A-X) spectra and to increase the reliability of the present gas temperature determinations. In order to show the small effect of $H_2$ admixture on the air plasma, figure 12 displays NO$\gamma$ spectra measured in the center of the nozzle of MW cavity (i.e. z=0) in the case of air plasma column with and without $H_2$ admixture under the same spectroscopic parameters (time exposure, distance between the plasma and the slit of spectrometer, etc.). It is noteworthy that NO$\gamma$ spectra are well representative of the thermal $O_2$ and $N_2$ dissociations and any non negligible variation of thermal plasma characteristics necessary affects NO$\gamma$ spectra. From the small difference observed in figure 12 between the two NO$\gamma$ spectra, we can conclude that the small $H_2$ admixture has a negligible effect on thermal characteristics of the present air plasma.

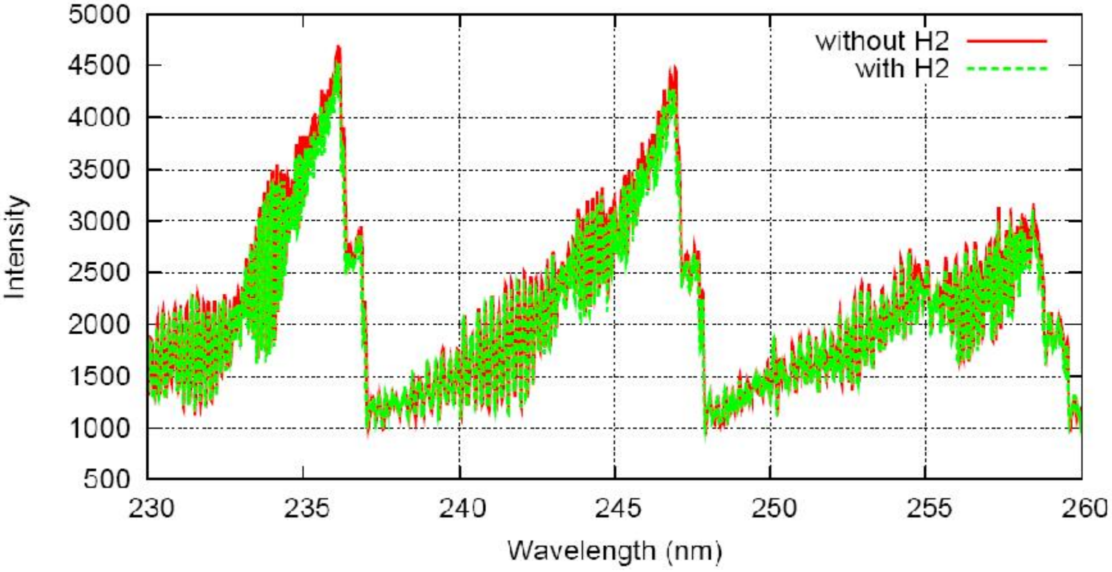

**Fig. 12. Measured NO$\gamma$ spectra of the air plasma column with and without a small amount of $H_2$ in the case of $P_{MW}$=1 kW, Pressure=600 mbar, and Gas flow=12 l/min.**

Gas temperature is determined from the best fit between measured and calculated OH(A-X) spectra since the rotation temperature is equivalent to the gas temperature. This is correct when the assumption of a quasi-instantaneous equilibrium between the rotation and the translation temperatures is fulfilled. The calculated or synthetic spectra are determined using Lifbase software [13]. However in order to simplify the methodology, we used the ratio $R_{IQIR}$ between the sum of intensity of Q1 (307.8 nm) and Q2 (308.9 nm) branches over the sum of intensity of R1 (306.36 nm) and R2 (306.77 nm) branches.

$$R_{I_Q I_R} = \frac{I_{Q1(307.8nm)} + I_{Q2(308.9nm)}}{I_{R1(306.36nm)} + I_{R2(306.77nm)}} \qquad (2)$$

This ratio $R_{IQIR}$ is first plotted versus a large range of gas temperature (see figure 12) using calculated OH(A-X) spectra. This then straightforwardly leads to the experimental estimation of the hot air plasma temperature by comparing the experimental ratio $R_{IQIR}$ to the plot of figure 13. This methodology is validated from a direct comparison of experimental and synthetic spectra for a given position of the air plasma column as displayed in the OH(A-X) spectra of figure 14 between 306 nm to 310 nm.

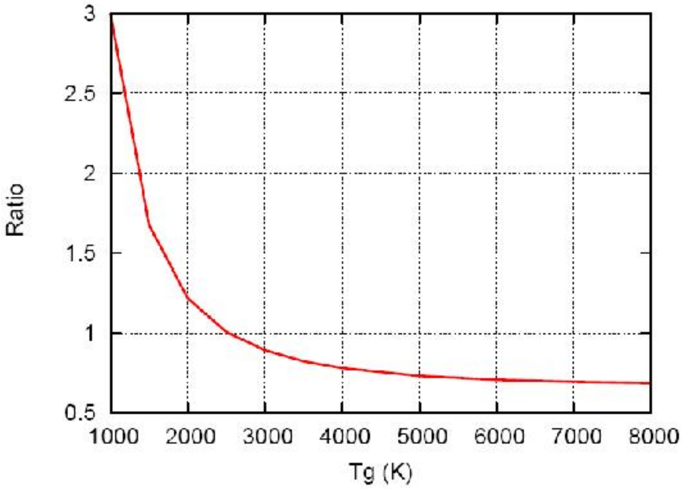

**Fig. 13. Variation versus the gas temperature of the ratio $R_{IQIR}$ of the intensities of Q1 and Q2 branches over the intensities of R1 and R2 branches in the case of synthetic spectra of OH(A-X) emissions**

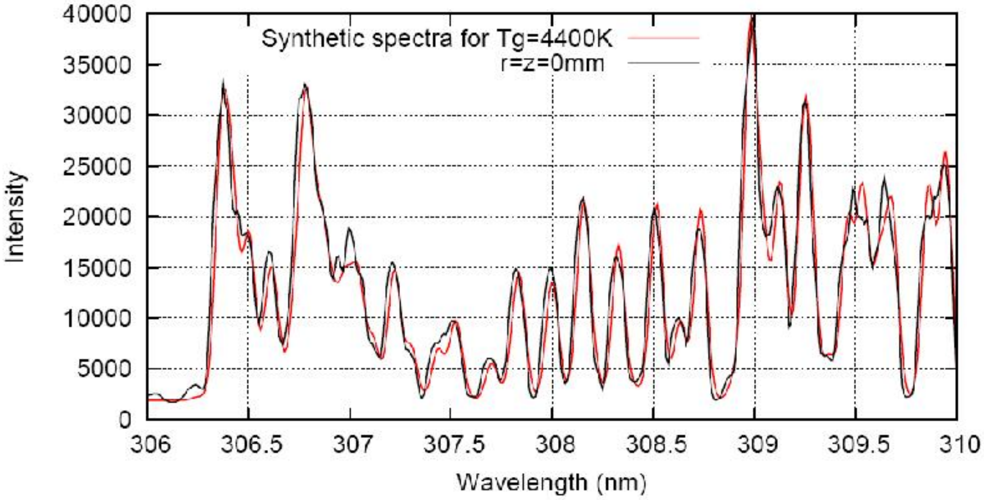

**Fig. 14. Comparison between experimental spectrum and calculated one for Tg=4400K at the position of plasma column: r=0, z=0 (in the center of plasma column and near the nozzle) in the case of $P_{MW}$=1 kW, Pressure=600 mbar, inlet gas composition=Air+3%$H_2$, and Gas flow=12 l/min.**

The measured gas temperatures along the axis of air plasma and the radial direction (at z=12m and 17mm corresponding to the TALIF position of atomic oxygen measurements) of the air plasma column are displayed in figures 15a and 15b.

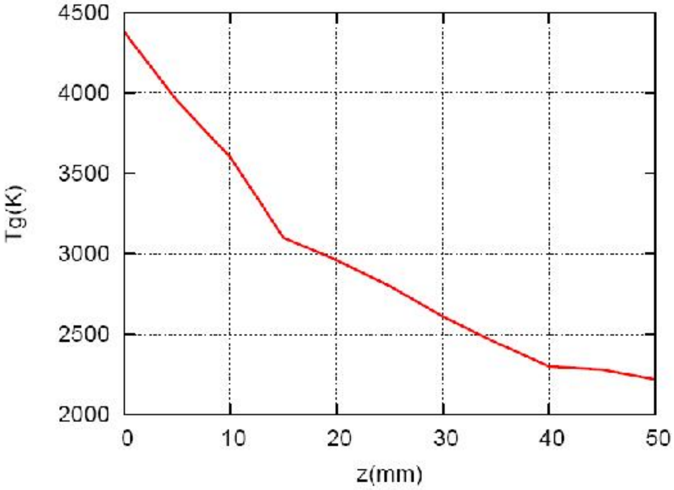

**Fig. 15a. Measured gas temperature along the axis of the air plasma column in the case of $P_{MW}$=1 kW, Pressure=600 mbar, inlet gas composition=Air+3%$H_2$, and Gas flow=12 l/min.**

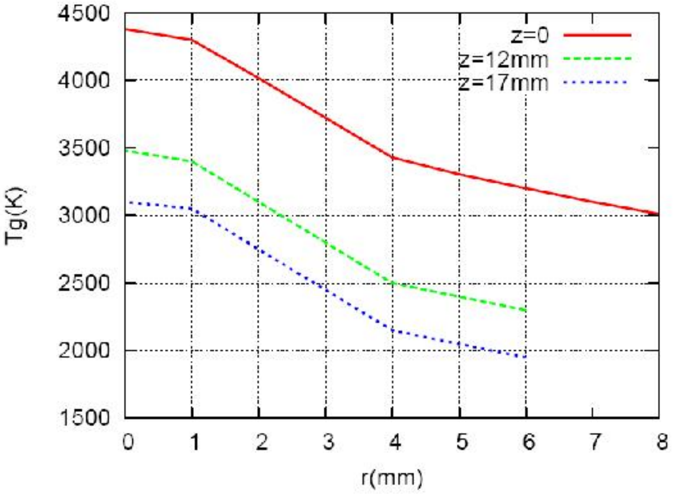

**Fig. 15b. Measured gas temperature along the radial direction of the air plasma column for 3 axial positions (z=0 near the nozzle of resonant cavity, z=1 mm and z=17 mm) in the case of $P_{MW}$=1 kW, Pressure=600 mbar, inlet gas composition=Air+3%$H_2$, and Gas flow=12 l/min.**

In order to know the dissociation of inlet molecular oxygen for the position in the air plasma column corresponding to the TALIF measurements of absolute atomic oxygen density, table 1 summarize the information on TALIF measurements, gas temperature and the corresponding molecular oxygen.

**Table 1. Summary of TALIF measurements of atomic oxygen density at different axial and radial positions of the hot air plasma column generated by microwave resonant cavity. The molecular density is determined from equation of the state at 600 mbar and the corresponding gas temperature Tg. Experimental conditions are: $P_{MW}$=1 kW, Pressure=600 mbar, inlet gas composition=Air+3%$H_2$, and Gas flow=12 liter/min.**

| | **r (mm)** | **TALIF O density ($cm^{-3}$)** | **Tg (K)** | **$O_2$ density ($cm^{-3}$) from p=NkTg** | **Density ratio [O]/[$O_2$** |
|---|---|---|---|---|---|
| **z=12mm** | **0** | **$(2.05\pm0.52)\times10^{17}$** | **3480** | **$2.50\times10^{17}$** | **0.82** |
| **z=17mm** | **0** | **$(1.23\pm0.31)\times10^{17}$** | **3100** | **$2.80\times10^{17}$** | **0.44** |
| | **1** | **$(1.16\pm0.29)\times10^{17}$** | **3050** | **$2.85\times10^{17}$** | **0.41** |
| | **2** | **$(0.64\pm0.16)\times10^{17}$** | **2750** | **$3.16\times10^{17}$** | **0.20** |
| | **3** | **$\approx0.05\times10^{17}$** | **2450** | **$3.55\times10^{17}$** | **≈0.01** |

Table 1 shows several interesting results:

- The decreasing radial profile of the atomic oxygen density is directly correlated to the decrease of gas temperature. The maximum density value is obviously in the axis of air plasma column where the gas temperature is the highest.
- The decreasing axial profile of the atomic oxygen density between z=12mm and z=17mm is also due to the gas temperature decrease along the axis the plasma column with increasing distance from the nozzle of microwave resonant cavity
- In comparison to an ideal concentration of molecular oxygen at a given pressure and temperature obtained from the state equation, the molecular dissociation is very important on the axis for z=12mm while this dissociation rapidly decreases versus the radial position at z=17mm before to become negligible. As a matter of fact the signal TALIF becomes too low to measure any atomic oxygen density for a radial position higher than 4mm at z=17mm corresponding to the border of the plasma column.
- the classical reactions of thermal dissociation are partly responsible of such behavior of atomic oxygen density since the gas temperature for which the ratio between atomic and molecular oxygen is close to unity can be estimated to 4000 K at 600 mbar (exactly Tg=3480K for ratio [O]/[$O_2$]=0.82 at z=12mm and r=0). While in the case of an air plasma assumed at local thermodynamic equilibrium (LTE), following the literature a temperature near 3000K is required to have the density ratio [O]/[$O_2$]=1. This means that the oxygen dissociation in such air plasma column, which behaves as a post-discharge, is lower than the thermal dissociation obtained under only local thermodynamic considerations. This also means that usual LTE (i.e. full micro-reversibility for the thermal processes where every forward reaction is balanced its backward one and thermal equilibrium between the different species of the plasma) are not fulfilled in the present air column plasma. In fact, the relaxation of some long-lived excited species (behaving as a tank of internal energy) is certainly not completely achieved when the air plasma is ejected from resonant cavity upward the gas conditioning cell. This is why the present air column plasma is not locally at thermal equilibrium at least in the region of the axis of the plasma column where the atomic oxygen density has been measured from TALIF spectroscopy.

## CONCLUSION

Further studies are planned to investigate the non-thermal equilibrium behavior of this post-discharge air plasma column by measuring more particularly the vibration, excitation and electron temperatures in order to better understand the non equilibrium properties of the present hot air plasma generated by microwave resonant cavity.

## ACKNOWLEDGEMENTS

The authors would like to thank CEA for the financial support of the whole setup of microwave resonant cavity.

## COMPETING INTERESTS

Authors have declared that no competing interests exist.

## REFERENCES

1. Niemi K, Schulz-von der Gathen V, Dobele H F. The role of helium metastable states in radio-frequency driven helium–oxygen atmospheric pressure plasma jets: measurement and numerical simulation. Plasma Sources Sci. Technol. 2005;14: 375–386

2. Georg A, Engemann J, Brockhaus A. Investigation of a pulsed oxygen microwave plasma by time-resolved two-photon allowed laser-induced fluorescence. J. Phys. D: Appl. Phys. 2002; 35: 875–881

3. Ono R, Yamashita Y, Takezawa K, Oda T. Behaviour of atomic oxygen in a pulsed dielectric barrier discharge measured by laser-induced fluorescence. J. Phys. D: Appl. Phys. 2005; 38: 2812–2816

4. Ono R, Takezawa K, Oda T. Two-photon absorption laser-induced fluorescence of atomic oxygen in the afterglow of pulsed positive corona discharge. J. Appl. Phys. 2009; 106: 043302

5. Reuter S, Winter J, Schmidt-Bleker A, Schroeder D, Lange H, Knake N, Schulz-von der Gathen V, Weltmann K-D. Atomic oxygen in a cold argon plasma jet: TALIF spectroscopy in ambient air with modelling and measurements of ambient species diffusion. Plasma Sources Sci. Technol. 2012; 21: 024005

6. Gupta M,Owano T, D Baer D, O'Keefe A. Quantitative determination of the O($^3P$) density via visible cavity-enhanced spectroscopy. APPLIED PHYSICS LETTERS 2006;89: 241503

7. Marchal F, Merbahi N, Ledru G, Gardou JP, Sewraj S. Study of VUV emissions of Ar2* excimers using three-photon absorption laser induced fluorescence. Journal of Physics B: Atomic, Molecular & Optical Physics, 2009; 42: 015201

8. Dilecce G, Vigliotti M and De Benedictis S. A TALIF calibration method for quantitative oxygen atom density measurement in plasma jets. J. Phys. D: Appl. Phys. 2000; 33:L53-L56

9. Kröll S, Bischel W K. Two photon absorption and photo-ionization cross section measurements in the 5p5 $^6$pconfiguration of xenon. Phys Rev A, 1990; 41:1340-1349

10.Saxon RP, Eichler J. Theoretical calculation of two photon absorption cross sections in atomic oxygen" Phys Rev A. 1986; 34:199-206

11. Ricard A, St-Onge L, Malvos H, Gicquel A, Hubert J, Moisan M. Torche à excitation micro-ondes: 2 configurations complémentaires. J.Phys III France. 1995; 5: 1269

12. Parigger C G, Guan G, Homkohl J O. Measurement and analysis of OH emission spectra following laser-induced breakdown in air. Applied Optics. 2003; 30:5986-5991

13. J. Luque and D. R. Crosley. LIFBASE: Database and spectral simulation program (version 1.5). SRI International Report No. MP 99(009), 1999